RSC Advances

PAPER

View Article Online
View Journal | View Issue

Cite this: *RSC Adv.*, 2023, **13**, 14729

Preparation of surface-modified electrode of copper(II) oxide mixed with the molecularly imprinted polymer for enhancement of melamine detection with photoelectrochemical technique

Dalawan Limthin,[a] Piyawan Leepheng,[a] Benchapol Tunhoo,[ab] Korakot Onlaor,[ab] Annop Klamchuen,[c] Darinee Phromyothin[a] and Thutiyaporn Thiwawong *[ab]

Melamine contamination in food and beverages affects short- and long-term health. In this work, enhanced sensitivity and selectivity in photoelectrochemical determination for melamine detection was achieved using copper(II) oxide (CuO) combined with a molecularly imprinted polymer (MIP). A CuO nanomaterial was used to achieve MIP surface modification *via* co-precipitation synthesis. An MIP film was deposited by polymerizing the methacrylic acid monomer and a melamine template. The properties of the CuO nanomaterials, such as the surface morphology, chemical oxidation state, and crystalline structure, were characterized using field emission scanning electron microscopy (FESEM), X-ray photoelectron spectroscopy (XPS), and X-ray diffraction patterns (XRD), respectively. The diffuse reflection spectroscopy technique was applied to evaluate the optical properties of the CuO nanoparticles. The results indicated that the synthesized CuO nanomaterials had a monoclinic structure with an optical bandgap of 1.49 eV, which corresponds to absorbance in the visible light region. CPE electrodes with surface-modified CuO/MIP were measured using the photoelectrochemical techniques of cyclic voltammetry, differential pulse voltammetry (DPV), and amperometry. The modified CuO/MIP electrode for melamine detection in 7.4 pH PBS buffer solution exhibited a high sensitivity of 0.332 nA nM^{-1}, with a linear range of 5.0–75.0 nM and a limit of detection of 2.45 nM. Moreover, real samples of various kinds of milk were applied to evaluate the sensing response of the prepared CuO/MIP electrode. The modified CuO/MIP electrodes could be reused seven times with good reproducibility and high selectivity for melamine detection.

Received 21st March 2023
Accepted 24th April 2023

DOI: 10.1039/d3ra01854g

rsc.li/rsc-advances

Introduction

Melamine is a triazine compound with a nitrogen-rich heterocyclic structure. Typically, melamine has been used to synthesize aminoplast resins and foam in the manufacture of coatings and packaging for food products.[1] This might lead to melamine contamination in food and beverages, which has harmful effects on short- and long-term health, such as nephrotoxicity and increased incidence of kidney stones.[2] In turn, this could result in organ failure, or, in the worst-case scenario, death. Therefore, the US Food and Drug Administration (FDA) determines the level of melamine concentration in food products and ensures a national safety limit of 0.63 mg kg^{-3}, and the World Health Organization (WHO) has defined a tolerable daily intake (TDI) level for melamine of 0.2 mg per kg per body mass.[2–4] To monitor food items and ensure their safety for consumption, it is crucial to develop quick and accurate melamine sensors.

Generally, several analytical techniques, such as high-performance liquid chromatography (HPLC),[5–7] liquid chromatography-mass spectrometry (LCMS),[6,8,9] gas chromatography-mass spectrometry (GCMS),[6,10–12] and fluorescence, among others, have been applied for melamine detection. These methods exhibited high selectivity and low limits of detection.[13,14] However, these techniques are expensive, time-consuming, and require complex specialists for use, limiting their practical application.

The photoelectrochemical method (PEC) is an analytical technique that combines electrochemical and photoelectric measurement processes using semiconductor materials.[15,16] This technique involves excitation with a light source to produce photogenerated electron–hole pairs in the nanomaterials. The photoelectrochemical method has been considered an alternative measurement technique to the previously

[a]*College of Materials Innovation and Technology, King Mongkut's Institute of Technology Ladkrabang, Bangkok, 10520, Thailand. E-mail: thutiyaporn.th@gmail.com*

[b]*Electronic and Control System for Nanodevice Research Laboratory (ECSN), College of Materials Innovation and Technology, King Mongkut's Institute of Technology Ladkrabang, 10520, Thailand*

[c]*National Nanotechnology Center, National Science and Technology Development Agency, Patumthani, 12120, Thailand*

used methods because of its various advantages, such as high sensitivity, low background interference, low limit of detection, and fast response.[16–18] It can be applied to portable devices for melamine detection. However, it has poor selectivity. This drawback can be overcome with surface modification of the working electrode. In the literature, many receptors, such as antibodies, aptamers, and enzymes, have been used in biosensors for selective detection.[19,20] However, they have weaknesses, such as low thermal stability, chemical stability, storage time, and stability under environmental conditions. Molecular imprinting techniques have been reported to overcome most of these drawbacks. Molecularly imprinted polymers (MIP) are synthetic polymeric materials produced *via* a polymerization method that produces specific cavities for a template molecule. The specific cavities formed in the MIP are compatible with the target analyte in terms of size, shape, and chemical function.[21–23] Therefore, MIPs are widely used in sensors for recognition of analytes such as pesticides, organic compounds, and biomolecules[21,22,24–29] because of their high selectivity, robust thermal and chemical stability, long storage time, ease of preparation, and low cost. However, MIPs are polymer matrices with low electrical conductivity; when an MIP is modified onto the surface of an electrode, it hampers charge transfer between the solution and electrode. This problem can be overcome with nanomaterials.

Photoactive nanomaterials generate electron–hole pairs material when interacting with light radiation. The charge transfer process in these materials can be improved by modifying working electrodes with nanostructure materials such as titanium dioxide (TiO_2),[30,31] bismuth sulfide (Bi_2S_3),[32,33] zinc oxide (ZnO),[34] tungsten trioxide (WO_3),[35] cerium dioxide (CeO_2),[36] La_2O_3@Cu_2S,[37] cupric oxide (CuO),[38,39] cuprous oxide (Cu_2O),[40] and graphitic carbon nitride (g-C_3N_4).[38,39] Among these, copper(II) oxide (CuO) is one of the promising materials of considerable interest, as it is a p-type semiconductor material with a monoclinic crystal structure and has a narrow energy band gap of 1.2–1.7 eV for higher visible and infrared light absorption.[41,42] Moreover, it shows environmental stability, thermal stability, good electrical conductivity, non-toxicity, low cost, abundance, and easy preparation. Previous works have reported various copper oxide synthesis processes, such as co-precipitation, sol–gel, green synthesis, microwave irradiation, electrochemical deposition, sonochemical, and biogenic methods. The co-precipitation process is a simple method with easy preparation and low cost, and can synthesize large batch sizes.[43] In addition, CuO has been reported for use in various applications including photovoltaic devices, gas sensors, supercapacitors, and photoelectrochemical water-splitting cells.[41,42,44,45]

In this work, a surface-modified electrode for melamine detection was fabricated using copper(II) oxide (CuO) mixed with molecularly imprinted polymers (CuO/MIP), which provided enhanced high sensitivity and selectivity. CuO was synthesized by the co-precipitation method using copper(II) nitrate hexahydrate as a precursor. The CuO/MIP electrode was fabricated using a polymerization method consisting of methacrylic acid (MAA) as a monomer. The behavior of the prepared electrode was characterized using the photoelectrochemical technique with the amperometry method, which demonstrated the performance of the electrode in melamine detection in terms of sensitivity, detection limit, and selectivity.

Experimental

Materials

Copper(II) nitrate hexahydrate (AR grade), methacrylic acid 99% (MAA), ethylene glycol dimethacrylate 98% (EGDMA), 0.2 M 2,2-azobisisobutyronitrile in toluene (AIBN), phosphate buffer saline (PBS, pH 7.4), uric acid (99% purity), thiourea (99% purity), ammonia 25%, and urea (99% purity) were purchased from Sigma-Aldrich. Melamine (99% purity), glycine (99% purity), sodium hydroxide (98.5% purity), chloroform (99.5% purity), and ethanol (99.8% purity) were purchased from Carlos. All reagents were of analytical grade. For real sample analysis, three milk types: cow milk, chocolate milk, and strawberry milk, were obtained from a local market (Bangkok, Thailand).

Preparation of copper(II) oxide nanomaterials

CuO was synthesized *via* the co-precipitation method, as shown in Fig. 1a.[46] In the first step, 0.50 M of the precursor copper(II) nitrate hexahydrate was dissolved in deionized (DI) water. Then, 1.0 M NaOH solution was slowly mixed in under stirring until the pH of the solution reached 14 and kept for 2 h. The colour of the synthesized solution changed from blue to black. The black precipitate particles were obtained and washed with DI water several times until the pH reached 7. Subsequently, the precipitated product was dried in an oven at 100 °C and calcined in a furnace at 350 °C for 4 h. The synthesized CuO nanoparticles were then kept in a dry desiccator.

Fabrication of CuO/MIP surface-modified electrode

A carbon plate electrode (CPE) was modified with CuO. 5.0 mg per mL CuO in 1% MAA was dropped on the CPE. After curing with UV irradiation for 15 min, the molecularly imprinted polymer was synthesized using a polymerization method involving melamine, MAA, EGDMA, and AIBN as the template,

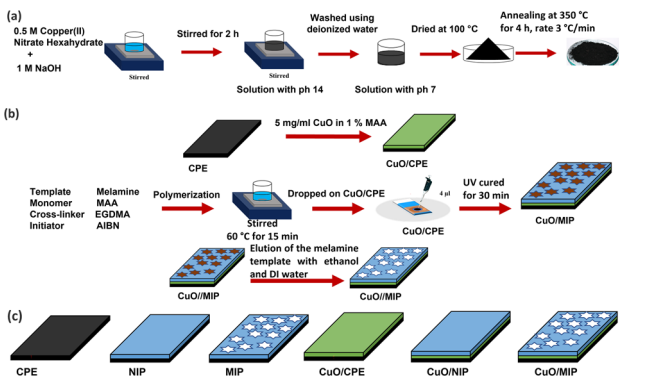

Fig. 1 Schematic diagram of the preparation process of the CuO nanomaterial (a), the preparation of the CuO/MIP-modified electrode (b), and models of the modified electrodes (c).

monomer, crosslinker, and initiator, respectively. The process of the surface modification of the electrodes is presented in Fig. 1b. First, 2.0 mL of 1.0 mM melamine was mixed with 1.0 mL of MAA dissolved in 2.5 mL chloroform. Then, AIBN and EGDMA were added to the mixture. MAA, EGDMA, and AIBN were mixed in a ratio of 1.0 : 5.0 : 0.5 by molarity at 60 °C for 30 min. Then, 3.0 μL of the precursor solution was dropped on the CuO/CPE electrode. The diameter of the circular working electrode was 3 mm, and the sensing area was 7.065 mm^2. The electrode was fixed with laminated Kapton tape and cured with a UV lamp for 30 min, forming a polymer matrix on the CuO/CPE electrode. Finally, the CuO/MIP electrode template was eluted with DI water and ethanol several times. The surface-modified electrode was dried and stored at room temperature in a desiccator. For comparison, six electrodes with different surface modifications, including carbon plate electrode (CPE) as a bare electrode, CuO-modified CPE (CuO/CPE), non-imprinted polymer (NIP), imprinted polymer (MIP), CuO combined with non-imprinted polymers (CuO/NIP), and CuO mixed with molecularly imprinted polymers (CuO/MIP) were studied, as presented in Fig. 1c.

Material characterizations

The CuO chemical composition purity and oxidation states were determined using X-ray photoelectron spectroscopy (XPS, Axis Ultra DLD, Kratos). X-ray diffraction (XRD, Smart lab, Rigaku) with a Cu Kα radiation source at an X-ray wavelength (λ) of 1.5406 Å was used to obtain the crystalline structure of the prepared CuO nanoparticles. The optical properties were observed using ultraviolet-visible-near infrared spectroscopy (UV-VIS-NIR spectrophotometer) (UH1450, HITACHI). The surface modification of the CuO/MIP electrodes on the modified surface was observed using an atomic force microscope (AFM, SPI3800N/SPA400, Seiko Instruments).

Electrochemical measurements

The melamine detection performance of the prepared device was analyzed *via* electrochemical measurements using a potentiostat (μSTAT 400, Dropsens) controlled by the computer program Dropview 8400. The measurement system was a tri-electrode measurement system that consisted of a 3 mm diameter carbon-paste electrode as the working electrode. The counter and the reference electrodes were carbon paste and silver/silver chloride. The photoelectrochemical characteristics of the sensing layer were determined using a measurement system under an excited xenon lamp irradiation with a power supply (Nikon Corporation: model C-FI 115), and the fixed intensity of the light was about 3 mW cm^{-2}. The various prepared electrodes were analyzed using cyclic voltammetry (CV) measurements in 50.0 mM potassium ferrocyanide in PBS buffer (pH = 7.4 at 25 °C). The applied voltage for the redox potential was set from −1.0 V to +1.0 V. In addition, the CuO/MIP electrode was tested with different melamine concentrations in PBS buffer. Differential pulse voltammetry was conducted with a potential range, scan rate, pulse width, and pulse amplitude of +0.2 V to −0.5 V, 20.0 mV s^{-1}, 50.0 ms, and 50.0 mV, respectively. Amperometry measurements were applied to investigate the performance of the CuO/MIP-modified electrodes using a fixed current at a voltage of −0.18 to execute and calculate the linear calibration curve, limit of detection, and sensitivity. The selectivity was analyzed using interference comparisons with fixed 100.0 nM concentrations each of glycine, uric acid, thiourea, ammonia, urea, and melamine solution.

Results and discussion

Copper(II) oxide synthesis

CuO was synthesized *via* the co-precipitate method using copper(II) nitrate hexahydrate as a precursor and calcined at 350 °C for 4 h. The surface morphology of CuO can be observed using high-magnification field emission scanning electron microscopy (FESEM), as shown in Fig. 3a. The sheet-like structure of the synthesized CuO particles showed that the particle thickness was smaller than the width dimension of the sheet-like particles. In Fig. 2, the chemical element purity and oxidation states of the CuO nanoparticles have been verified using X-ray photoelectron spectroscopy (XPS). The XPS survey spectrum of CuO established the presence of peaks associated with the elements Cu, O, and C, as shown in Fig. 2a. Fig. 2b–d show the high-resolution spectra with deconvolution in the XPS peaks of Cu 2p, O 1s, and C 1s, respectively. The XPS of Cu 2p is presented in Fig. 2b, which confirms the existence of Cu^{2+}; two energy peaks were present at 953.5 eV and 933.4 eV, corresponding to Cu $2p_{1/2}$ and Cu $2p_{3/2}$, respectively. The two peaks at 963 eV and 942 eV are the satellite peaks of Cu $2p_{1/2}$ and Cu $2p_{3/2}$, respectively. They demonstrate the presence of the incomplete 3d orbital, further demonstrating the existence of Cu^{2+} in the sample. The atomic ratio of O/Cu was 1.27, and the prominent shake-up peak at the higher binding energy side of Cu $2p_{3/2}$ can be attributed to the formation of the CuO material.[47,48] In Fig. 2c, the high-resolution XPS spectra of O 1s for CuO presents a peak at 529.8 eV, which is stronger and

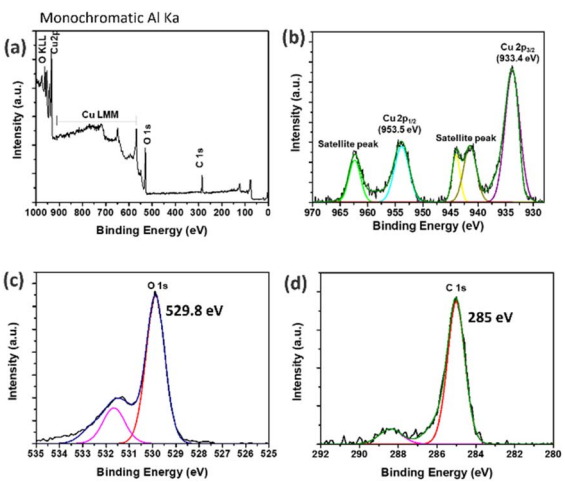

Fig. 2 Survey XPS spectrum (a) and high-resolution Cu 2p (b), O 1s (c), and C 1s (d) XPS spectra.

associated with the binding energy for lattice oxygen O^{2-} in CuO lattice. Fig. 2d shows the high-resolution XPS spectrum of C 1s. The peak at 285 eV was confirmed to be the C reference peak. Thus, the XPS spectrum of CuO has also established no residual contamination.

The crystallinity of the synthesized CuO nanomaterials was confirmed using X-ray diffraction (XRD). Fig. 3b presents the XRD pattern of the sample, in which the sharp diffraction peaks observed at 2θ values of 32.59°, 35.61°, 38.78°, 48.82°, 53.54°, 58.37°, 61.60°, 66.31°, and 68.15° were assigned to (1 1 0), (0 0 2), (1 1 1), (−2 0 2), (0 2 0), (2 0 2), (−1 1 3), (−3 1 1), and (2 2 0), in good agreement with JCPDS standard no. 45-0937. The main diffraction peak was that of the (002) plane with the monoclinic phase structure of CuO. Moreover, no impurity peaks of other material phases were observed, indicating the high purity of the synthesized product. The crystallite size can be calculated using the Debye–Scherrer equation[49] below:

$$D = \frac{\kappa\lambda}{\beta \cos\theta} \quad (1)$$

where κ is a constant value (0.9), λ is the wavelength of the X-ray source (1.5406 Å), and β is the full width at half maximum (FWHM), and θ is the diffraction angle, respectively. The calculated crystalline grain size was 21.35 nm, which indicated the nanostructure of the CuO material.

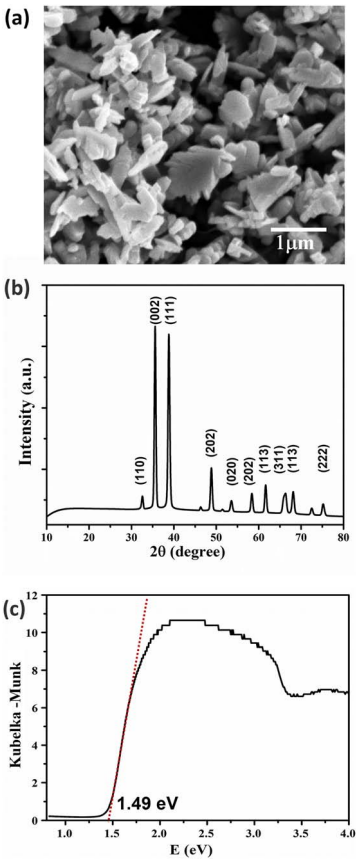

Fig. 3 Characterization of CuO: surface morphology observed using FESEM (a), XRD pattern (b), and Kubelka–Munk plot (c).

Therefore, the CuO nanomaterial can be synthesized *via* the co-precipitation method, which was confirmed from the monoclinic structure from the XPS and XRD results. The sample's optical properties were analyzed using the diffuse reflection technique and calculated using the Kubelka–Munk relation. The obtained energy bandgap is 1.49 eV, and thus a light source in the visible light range can be used to operate the prepared device.

Determining the optical band gap energy is crucial for optimizing the generated electron–hole pairs in semiconductor materials under light illumination. The diffuse reflection method was used to examine the optical behaviours of the CuO nanoparticles. In the reflection spectra, the *x*-axis intercept of the straight line equation was used to calculate the related optical band gap using the Kubelka–Munk equation.[50]

$$F(R) = \frac{(1-R)^2}{2R} \quad (2)$$

where R is the diffuse reflectance. It was found that the CuO nanomaterials presented a copper(II) oxide narrow band gap of 1.49 eV, as shown in Fig. 3c. The minimum wavelength required to promote electron transition from the valence to the conduction band was 832 nm, which represents visible light absorption.

Surface modified electrode

The CuO/MIP, fabricated by modifying a carbon plate electrode with copper(II) oxide combined with a molecularly imprinted polymer, presented specific cavities for melamine detection because of the elution process of the melamine template. Fig. 4 depicts images of the modified surfaces obtained using atomic force microscopy, comparing the CuO/NIP and CuO/MIP electrodes. The CuO/NIP electrode was almost flat with a surface roughness of about 69.67 nm, whereas CuO/MIP showed a rough surface with an RMS value of 110.64 nm. The AFM image of the CuO/MIP electrode indicates a higher surface roughness compared to the CuO/NIP electrode. The rough surface signatures of MIP correspond to the formation of cavities due to the eluted templates.

The electrochemical analysis was conducted for the different modified electrodes, which comprised six electrode models: a carbon plate electrode as a bare electrode, and a CuO/CPE, NIP, MIP, CuO/NIP, and CuO/MIP electrode. The modified electrodes were measured in CV mode, presenting a redox reaction of potassium ferricyanide in the −1 V to 1 V voltage range, as shown in Fig. 5a. The CuO/CPE electrode exhibited the

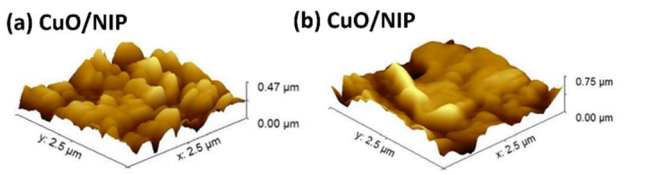

Fig. 4 Three-dimensional (3D) AFM images of CuO/NIP (a) and CuO/MIP (b).

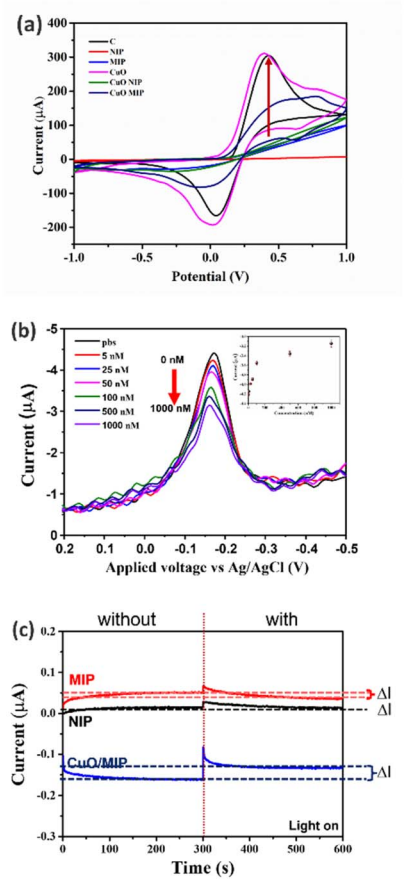

Fig. 5 Response analysis of surface-modified electrodes: cyclic voltammogram of the different modified electrodes using 0.05 M ($[K_4Fe(CN)_6]$) in 0.1 M PBS (a), differential pulse voltametric response in different concentrations of melamine at 0–100.0 nM (b), relationship between the DPV current and melamine concentration (inset) and amperometry current response of 100.0 nM melamine with different modified electrodes (c) using a constant light intensity of 3 mW cm^{-2}.

highest current signal, followed by CPE, CuO/MIP, CuO/NIP, MIP, and NIP, respectively. In the results, the MIP electrode showed higher current than the NIP electrode because the template elution of the MIP electrode created cavities that led to a high surface area, facilitating charge transfer. In contrast, the NIP electrode was smooth and thick, resulting in low current.

Moreover, the CuO/MIP-modified electrode exhibited a higher response than the MIP-modified electrode. This might be because CuO has good electrical conductivity and carrier mobility properties that improved the charge transfer. In addition, the CuO/MIP electrode was tested with melamine solution and measured using the differential pulse voltametric method in the 0.2 V to −0.5 V range. In the differential pulse voltametric response at different melamine concentrations, the potential switching scan to more negative presented a reduction reaction, and a cathodic peak signal was observed at an applied potential of −0.18 V. Increasing melamine concentration corresponded with a decrease in the current of the cathodic signal, as shown in Fig. 5b. The applied potential was fixed at −0.18 V for the amperometry analysis. In addition, the inset of Fig. 5b depicts the relationship between the DPV current and melamine concentration, which demonstrated a nonlinear relationship. In addition, the CuO/MIP-modified electrodes were used and analyzed for melamine detection in amperometry mode at −0.18 V for 600 s. The performance between the NIP, MIP, and CuO/MIP electrodes was compared. As shown in Fig. 5c, the CuO/MIP-modified electrode presented a difference in its current signal between before and after melamine recognition, with its greatest ΔI value indicating the highest signal. At the same time, the MIP and NIP electrodes exhibited a slight difference. The NIP and MIP are polymer matrices and insulators, which hampers charge transfer between the solution and electrode. In contrast, the CuO/MIP electrode consists of CuO, which has good electrical conductivity and increases charge transfer.

Effect of light irradiation

The electrochemical analysis was conducted at different melamine concentrations using amperometry, and the response of the CuO/MIP electrode in the presence of different melamine concentrations is presented under light and dark conditions at a constant light intensity of 3 mW cm^{-2}. The CuO/MIP electrode presented a reduction reaction, which increased the cathodic current under visible light irradiation. The current signal in the dark conditions demonstrated a lower signal, as shown in Fig. 6a. The increase in the cathodic current was found due to the CuO material being a photoactive material and p-type semiconductor, which presented an energy bandgap of 1.49 eV correlating to the optical absorption and generating electron–hole pairs in the visible light region. The electrons participated in interfacial electron transfer reactions to reduce water to hydrogen and the holes transferred from the cathode to the anode. Thus, CuO can enhance the charge transfer of the modified electrodes under visible light absorption.

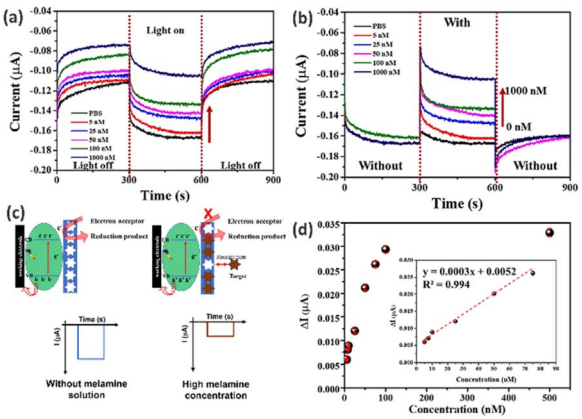

Fig. 6 Amperometry current response of the CuO/MIP electrode under light on–off conditions (a) and with removing and rebinding of the template (b) at different melamine concentrations. Model of the photoelectrochemical detection mechanism of the CuO/MIP-modified electrode (c) and the response curve and standard calibration plot (inset) for the detection of melamine using CuO/MIP (d).

Performance of CuO/MIP surface-modified electrode

The performance of the CuO/MIP-modified electrode was measured using electrochemical techniques under light irradiation. Fig. 6b indicates that increasing melamine concentration led to a fall in the cathodic current. This occurred because the melamine target was recognized in the cavities of the MIP, which hindered charge transfer between the solution and electrode, as shown in the model of the photoelectrochemical melamine detection mechanism of the CuO/MIP-modified electrodes depicted in Fig. 6c.

Fig. 6d depicts the calibration curve between the melamine concentration and electrode current. The relationship between the current and concentration of melamine was considered in the range of 5.0–500.0 nM. Increasing melamine concentration resulted in an increase in ΔI, and the signal value changed only slightly above a concentration of 100.0 nM. The linearity of the calibration plot showed the relationship between the delta current and the concentration of melamine, and a linear response was observed in the range of 5.0–75.0 nM with the linear equation $y = 0.0003x + 0.0052$, where y is the delta current (μA) and x is the melamine concentration (nM); the correlation coefficient was 0.994. Moreover, the sensitivity of melamine detection was presented as 0.332 nA nM^{-1}, and the limit of detection (LOD) was 2.45 nM. Generally, the LOD can be calculated as LOD = 3.3 × (S. D.)/M, where S. D. is the standard deviation of the response, and M is the slope of the calibration curve. Furthermore, the limit of melamine detection for the CuO/MIP electrode was lower than the FDA and WHO levels at a concentration of 2.5 mg kg^{-1}. Therefore, the fabricated CuO/MIP electrode represents a candidate for the sensing layer following the specifications of the FDA and WHO.

Reproducibility and reusability

The CuO/MIP electrode was tested for reproducibility and reusability. Table 1 presents the data for the six surface-modified electrodes; they demonstrated similar values for both sensitivity and limit of detection because the modified electrode defined the area and process of preparing the working electrode. Thus, this process is stable and can be reproducible. As shown in Fig. 7a, the reusability of the CuO/MIP electrode was tested ten times using a melamine concentration of 100.0 nM, and was found to be reusable seven times. The modified electrode repeatedly eluted the template in melamine detection, causing polymer defects, including cracking and swelling. The decrease of the current, as seen in the eighth cycle, is an indication of the presence of melamine.

Table 1 Reproducibility of CuO/MIP-modified electrode for melamine detection

Electrode	Linear equation	R^2	Sensitivity (nA nM^{-1})	LOD (nM)
1	$y = 0.0003x + 0.0052$	0.994	0.332	2.45
2	$y = 0.0003x + 0.0057$	0.994	0.326	2.50
3	$y = 0.0003x + 0.0067$	0.997	0.350	2.24
4	$y = 0.0003x + 0.0055$	0.991	0.320	2.44
5	$y = 0.0003x + 0.0047$	0.993	0.296	2.23
6	$y = 0.0003x + 0.0058$	0.993	0.325	2.46

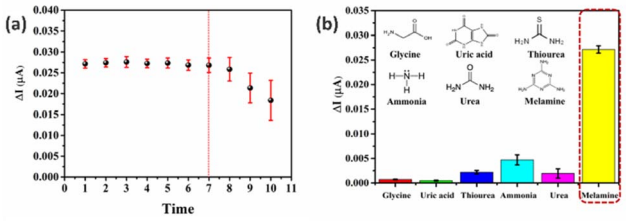

Fig. 7 The responses of the CuO/MIP electrode in tests of its reusability for melamine detection (a) and its selectivity to different compounds such as glycine, uric acid, thiourea, ammonia, urea, and melamine (b).

Selectivity

The surface-modified electrodes were fabricated using CuO mixed with MIP. Solutions of interferents, namely, glycine, uric acid, thiourea, ammonia, urea, and melamine, were used to test the selectivity of the CuO/MIP electrode. A strong signal was demonstrated in the association of melamine sensing response on the CuO/MIP electrode. Other interferents presented a low signal, as shown in Fig. 7b. Thus, the CuO/MIP electrode exhibits good selectivity for melamine detection. This might be due to the specific affinity provided by the MIP technique, that is, the removal of the template in the MIP electrode from the polymer created specific cavities with a molecular memory targeting melamine molecules, based on characteristics such as their size, shape, and functional groups.

Melamine molecules are nitrogen-rich heterocyclic triazine compounds, and the functional monomer of MAA is an acidic functional group containing a carboxyl moiety. Thus, the amino groups of melamine can interact with the carboxyl group of the MAA monomer through hydrogen bonding, electrostatic interactions, and van der Waals forces.[51–53]

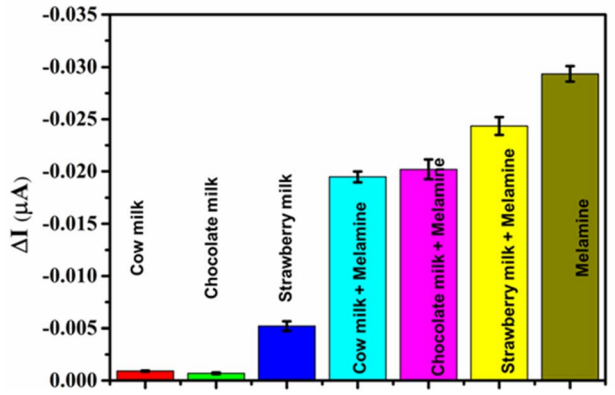

Fig. 8 Responses of the CuO/MIP electrode in real samples, namely, cow milk, chocolate milk, strawberry milk, melamine-contaminated cow milk, melamine-contaminated chocolate milk, melamine-contaminated strawberry milk, and melamine.

Table 2 Comparison of the modified CuO/MIP electrode for melamine detection with other methods

Method	Material	Linear range (μM)	LOD (μM)	Ref.
HPLC-MS/MS	—	0.020–5	0.05	11
Quartz crystal microbalances	MIP	1–320	8	52
Electrochemistry	Poly(*para*-amino-benzoic acid)/GCE	4–450	0.36	54
Electrochemistry	MIL-101/AuNPs/CTS-PVP-rGO/GCE	5×10^{-5} to 1×10^{-2}	5×10^{-5}	55
Electrochemistry	CNT/MIP	0.4–9.2	0.11	56
Photo electrochemistry	CuO/MIP	0.005–50	0.00245	This work

Real sample measurement

The CuO/MIP electrode was analyzed using seven real samples: cow milk, chocolate milk, strawberry milk, melamine-contaminated cow milk, melamine-contaminated chocolate milk, and melamine-contaminated strawberry milk, and melamine. The melamine-contaminated samples exhibited significant change in the signal, whereas the non-contaminated samples showed only slight changes in the signal because the CuO/MIP electrode was sensitive to melamine detection in real samples. Thus, it can be seen that the CuO/MIP electrode shows high sensitivity and selectivity for melamine detection as shown in Fig. 8.

Table 2 compares the melamine detection in this work with that in other works with various materials, methods, and performances. HPLC-MS/MS[11] shows high selectivity and a significant detection limit, but this method is complex for users, limiting its practical application. Quartz crystal microbalances modified with MIP[52] have high selectivity, but this method is hard to control because it is sensitive to mass and perturbed by the environment. In comparison, the electrochemical process was used for melamine because of various advantages, such as high sensitivity, low limit of detection, fast response and applicability to portable melamine detection devices. The sensitivity of melamine detection was improved by the nanomaterial properties, which led to the charge transfer process. Advanced materials such as MIL 101, CNTs, *etc.*,[54–56] were used for enhanced sensitivity, but these materials are expensive and have complicated synthesis processes. It can be seen that the charge transfer in the photoelectrochemical process can be improved using CuO nanomaterial. Thus, CuO nanomaterial combined with MIP was used for melamine detection, and presented high sensitivity, high selectivity, a low limit of detection, and a wide linear range.

Conclusion

In conclusion, a photoelectrochemical method for detecting melamine with the fabrication of a novel surface-modified Cu/MIP electrode was developed. CuO nanoparticles were synthesized *via* the co-precipitate method and presented a monoclinic structure and a narrow energy bandgap of 1.49 eV. This indicates that they are a photoactive material and generate electron–hole pairs when interacting with visible light, and can be used for surface modification of the electrode to improve charge transfer. The CuO/MIP-modified electrode was tested using electrochemical techniques under light irradiation. The modified electrode exhibited good characteristics with high sensitivity, a wide linear range, good reproducibility, and reusability for more than seven cycles for melamine detection. The detection limit was 2.45 nM, which is lower than the FDA and WHO limits (2.5 mg kg^{-1}). In addition, there was high selectivity for melamine detection because of the specific cavities of the MIP. This CuO/MIP-modified electrode was designed and applied to the photoelectrochemical detection melamine and could be developed into a portable device. It is applicable to the detection of food contamination.

Conflicts of interest

There are no conflicts to declare.

Acknowledgements

The authors acknowledge the facilities and technical assistance from Nanotechnology and Materials Analytical Instrument Service Unit (NMIS) of College of Materials Innovation and Technology, King Mongkut's Institute of Technology Ladkrabang.

References

1 K. Bischoff, in *Reproductive and Developmental Toxicology*, ed. R. C. Gupta, 2nd edn, 2017, pp. 493–501.
2 Y. C. Tyan, M. H. Yang, S. B. Jong, C. K. Wang and J. Shiea, *Anal. Bioanal. Chem.*, 2009, **395**, 729–735.
3 J. R. Ingelfinger, *N. Engl. J. Med.*, 2008, **359**, 2745–2748.
4 C. M. Gossner, J. Schlundt, P. Ben Embarek, S. Hird, D. Lo-Fo-Wong, J. J. Beltran, K. N. Teoh and A. Tritscher, *Environ. Health Perspect.*, 2009, **117**, 1803–1808.
5 A. Filazi, U. T. Sireli, H. Ekici, H. Y. Can and A. Karagoz, *J. Dairy Sci.*, 2012, **95**, 602–608.
6 Y. Liu, E. E. Todd, Q. Zhang, J. R. Shi and X. J. Liu, *J. Zhejiang Univ., Sci., B*, 2012, **13**, 525–532.
7 X. Ge, X. Wu, S. Liang and H. Sun, *J. Chromatogr. Sci.*, 2013, **52**, 751–757.
8 M. Ibáñez, J. V. Sancho and F. Hernández, *Anal. Chim. Acta*, 2009, **649**, 91–97.
9 P. Panuwet, J. V. Nguyen, E. L. Wade, P. E. D'Souza, P. B. Ryan and D. B. Barr, *J. Chromatogr. B: Anal. Technol. Biomed. Life Sci.*, 2012, **887–888**, 48–54.
10 X.-m. Xu, Y.-p. Ren, Y. Zhu, Z.-x. Cai, J.-l. Han, B.-f. Huang and Y. Zhu, *Anal. Chim. Acta*, 2009, **650**, 39–43.

11 Y.-T. Wu, C.-M. Huang, C.-C. Lin, W.-A. Ho, L.-C. Lin, T.-F. Chiu, D.-C. Tarng, C.-H. Lin and T.-H. Tsai, *J. Chromatogr. A*, 2009, **1216**, 7595–7601.
12 H. Miao, S. Fan, Y. N. Wu, L. Zhang, P. P. Zhou, J. G. Li, H. J. Chen and Y. F. Zhao, *Biomed. Environ. Sci.*, 2009, **22**, 87–94.
13 L. Guo, J. Zhong, J. Wu, F. Fu, G. Chen, Y. Chen, X. Zheng and S. Lin, *Analyst*, 2011, **136**, 1659–1663.
14 Q. Du, F. Qu, B. Mao, S. Zhu and J. You, *New J. Chem.*, 2016, **40**, 8459–8464.
15 G. Wang, J. Xu and H. Chen, *Sci. China, Ser. B: Chem.*, 2009, **52**, 1789.
16 J. Shu and D. Tang, *Anal. Chem.*, 2020, **92**, 363–377.
17 A. Devadoss, P. Sudhagar, C. Terashima, K. Nakata and A. Fujishima, *J. Photochem. Photobiol., C*, 2015, **24**, 43–63.
18 I. Ibrahim, H. N. Lim, R. Mohd Zawawi, A. Ahmad Tajudin, Y. H. Ng, H. Guo and N. M. Huang, *J. Mater. Chem. B*, 2018, **6**, 4551–4568.
19 N. Bhalla, P. Jolly, N. Formisano and P. Estrela, *Essays Biochem.*, 2016, **60**, 1–8.
20 N. A. Parmin, U. Hashim, S. C. B. Gopinath and M. N. A. Uda, in *Nanobiosensors for Biomolecular Targeting*, ed. S. C. B. Gopinath and T. Lakshmipriya, 2019, pp. 195–210.
21 J. J. BelBruno, *Chem. Rev.*, 2019, **119**, 94–119.
22 Z. El-Schich, Y. Zhang, M. Feith, S. Beyer, L. Sternbæk, L. Ohlsson, M. Stollenwerk and A. G. Wingren, *BioTechniques*, 2020, **69**, 406–419.
23 E. Turiel and A. M. Esteban, in *Solid-Phase Extraction*, ed. C. F. Poole, 2020, pp. 215–233.
24 D. Limthin, K. Chattrairat, P. Leepheng, S. Wisutthipat, P. Gansa, A. Klamchuen and D. Phromyothin, *J. Met., Mater. Miner.*, 2019, **29**, 42–48.
25 D. Limthin, A. Klamchuen and D. Phromyothin, *Ferroelectrics*, 2019, **552**, 97–107.
26 P. Leepheng, D. Limthin, K. Onlaor, B. Tunhoo, D. Phromyothin and T. Thiwawong, *Jpn. J. Appl. Phys.*, 2021, **60**, SCCJ03.
27 P. Leepheng, D. Limthin, K. Onlaor, B. Tunhoo, T. Thiwawong, S. Suramitr and D. Phromyothin, *Jpn. J. Appl. Phys.*, 2022, **61**, SD1009.
28 D. Limthin, P. Leepheng, A. Klamchuen and D. Phromyothin, *Polymers*, 2022, **14**, 91.
29 D. Limthin, P. Leepheng, K. Onlaor, B. Tunhoo, A. Klamchuen, T. Thiwawong and D. Phromyothin, *Jpn. J. Appl. Phys.*, 2022, **61**, SD1033.
30 K. Arifin, R. M. Yunus, L. J. Minggu and M. B. Kassim, *Int. J. Hydrogen Energy*, 2021, **46**, 4998–5024.
31 X. Huang, R. Zhang, X. Gao, B. Yu, Y. Gao and Z.-g. Han, *Int. J. Hydrogen Energy*, 2021, **46**, 26358–26366.
32 J. Chao, S. Xing, Y. Zhao, S. Gao, Q. Song, L. Guo, D. Wang and T. Zhang, *Solid State Sci.*, 2016, **61**, 51–57.
33 B. Sun, T. Feng, J. Dong, X. Li, X. Liu, J. Wu and S. Ai, *CrystEngComm*, 2019, **21**, 1474–1481.
34 N. Abdullayeva, C. T. Altaf, M. Mintas, A. Ozer, M. Sankir, H. Kurt and N. D. Sankir, *Sci. Rep.*, 2019, **9**, 11006.
35 J. Huang, P. Yue, L. Wang, H. She and Q. Wang, *Chin. J. Catal.*, 2019, **40**, 1408–1420.
36 E. Kusmierek, *Catalysts*, 2020, **10**, 1435.
37 M. M. Foroughi and S. Jahani, *Microchem. J.*, 2022, **179**, 107546.
38 J. Safaei, N. A. Mohamed, M. F. Mohamad Noh, M. F. Soh, N. A. Ludin, M. A. Ibrahim, W. N. Roslam Wan Isahak and M. A. Mat Teridi, *J. Mater. Chem. A*, 2018, **6**, 22346–22380.
39 H. Wang, Y. Xu, D. Xu, L. Chen, X. Qiu and Y. Zhu, *ACS ES&T Engg*, 2022, **2**, 140–157.
40 M. M. Foroughi, S. Jahani, Z. Aramesh-Broujeni and M. Rostaminasab Dolatabad, *RSC Adv.*, 2021, **11**, 17514–17525.
41 R. Tomita, Z. Pu, T. Kamegawa, M. Anpo and S. Higashimoto, *Res. Chem. Intermed.*, 2019, **45**, 5947–5958.
42 R. Siavash Moakhar, S. M. Hosseini-Hosseinabad, S. Masudy-Panah, A. Seza, M. Jalali, H. Fallah-Arani, F. Dabir, S. Gholipour, Y. Abdi, M. Bagheri-Hariri, N. Riahi-Noori, Y.-F. Lim, A. Hagfeldt and M. Saliba, *Adv. Mater.*, 2021, **33**, 2007285.
43 P. Raizada, A. Sudhaik, S. Patial, V. Hasija, A. A. Parwaz Khan, P. Singh, S. Gautam, M. Kaur and V.-H. Nguyen, *Arabian J. Chem.*, 2020, **13**, 8424–8457.
44 Y. S. Chaudhary, A. Agrawal, R. Shrivastav, V. R. Satsangi and S. Dass, *Int. J. Hydrogen Energy*, 2004, **29**, 131–134.
45 J. Li, X. Jin, R. Li, Y. Zhao, X. Wang, X. Liu and H. Jiao, *Appl. Catal., B*, 2019, **240**, 1–8.
46 A. Muthuvel, M. Jothibas and C. Manoharan, *Nanotechnol. Environ. Eng.*, 2020, **5**, 14.
47 D. Barreca, A. Gasparotto and E. Tondello, *Surf. Sci. Spectra*, 2007, **14**, 41–51.
48 M. A. Khan, N. Nayan, Shadiullah, M. K. Ahmad and C. F. Soon, *Nanomaterials*, 2020, **10**, 1298.
49 U. Holzwarth and N. Gibson, *Nat. Nanotechnol.*, 2011, **6**, 534.
50 J. Militký, in *Soft Computing in Textile Engineering*, ed. A. Majumdar, 2011, pp. 45–102.
51 X. Ge, X. Wu, J. Wang, S. Liang and H. Sun, *J. Dairy Sci.*, 2015, **98**, 2161–2171.
52 M. Zeilinger, H. Sussitz, W. Cuypers, C. Jungmann and P. Lieberzeit, *Sensors*, 2019, **19**, 2366.
53 S. Farooq, H. Wu, J. Nie, S. Ahmad, I. Muhammad, M. Zeeshan, R. Khan and M. Asim, *Sci. Total Environ.*, 2022, **804**, 150293.
54 Y. T. Liu, J. Deng, X. L. Xiao, L. Ding, Y. L. Yuan, H. Li, X. T. Li, X. N. Yan and L. L. Wang, *Electrochim. Acta*, 2011, **56**, 4595–4602.
55 Z. Ruichi, S. Sun, W. Hao, H. Guo, Y. Gao and L. Shi, *Russ. J. Electrochem.*, 2019, **55**, 651–662.
56 B. Liu, B. Xiao, L. Cui and M. Wang, *Mater. Sci. Eng., C*, 2015, **55**, 457–461.